MATERIALS AND INTERFACES

Coating of Metal Powders with Polymers in Supercritical Carbon Dioxide

Evgeni M. Glebov, Li Yuan, Larisa G. Krishtopa, Oleg M. Usov, and Lev N. Krasnoperov*

Department of Chemical Engineering, Chemistry and Environmental Science, New Jersey Institute of Technology, Newark, New Jersey 07102

Supercritical carbon dioxide was used as a solvent to produce polymeric films on fused silica plates and metal (Al, Mg) powders. Two polymers, poly(vinylidene fluoride) and poly(4-vinylbiphenyl) (PVB), were used. Polymer-coated particles of metal powders exhibit enhanced resistance to the dissolution in aqueous basic and acidic solutions. The protective properties of the films were quantified based on the dissolution rate. The average thickness of the PVB films (that contain aromatic rings) was evaluated using UV absorption spectroscopy. A technique to measure the solubilities of poorly soluble polymers in supercritical carbon dioxide was developed. The effect of the coating conditions on the protective properties of the produced polymeric films was evaluated.

I. Introduction

Supercritical fluids exhibit a number of properties that make them attractive substitutes of organic solvents in a variety of chemical technological processes. Because of the strong dependence of the solubilities, transport, and other properties on pressure near the critical conditions, both temperature and pressure could be used as efficient process control parameters.[1,2] Among supercritical fluids, supercritical carbon dioxide (SC CO_2) is of particular interest. Supercritical carbon dioxide is an "environmentally benign" solvent.[1,2] It has a low critical temperature ($T_c = 304.2$ K) and a moderate critical pressure ($p_c = 72.8$ atm). SC CO_2 represents a prospective medium for a number of chemical engineering processes, such as extraction,[3] precise cleaning,[4] and chemical reactions[1,5] (including polymer synthesis[6,7]). Carbon dioxide is not an ozone-depleting compound and can be recycled by simple compression−decompression steps. Because of these properties, carbon dioxide is a very attractive potential solvent for the technological processes with a near-zero waste production. In addition, carbon dioxide is nontoxic, nonflammable, and inexpensive and does not represent a volatile organic compound (VOC) as defined by the U.S. Environmental Protection Agency.

One of the prospective applications of supercritical fluids is in the coating of solid powders with thin films.[8−11] Metal powders are common components of the pyrotechnic and the solid propellant compositions.[12] Coating of metal powders reduces their deterioration through corrosion and aggregation caused by moisture or other aggressive surroundings.[13] Coating of metal nanoparticles with polymers also reduces their flammability and makes them safe to handle.[14] The technologies currently used in the industry for coating of solid substrates, such as the Wurster coating process[15] or fluidized-bed coating,[16] employ common organic solvents. Replacement of organic solvents with SC CO_2 could result in an alternative, environmentally friendly approach.

The application of supercritical fluids for coating of solid substrates is based on the strong effects of pressure and temperature on the solubilities of the low-volatile compounds in supercritical fluids. Formation of solid particles upon decompression of supercritical fluid solutions was observed more than a century ago.[17] More recently, formation of fine particles during the expansion of solutions in SC CO_2 through a valve was observed for a number of different solutes.[18−21] Further development of this approach is the rapid expansion of supercritical solution (RESS) technique,[3,22−29] in which a supercritical solution (or suspension[30]) is expanded across a fine throttling device, such as a capillary or a nozzle.

While the majority of the research was focused on the production of fine particles of pure compounds using supercritical solution expansion, there have been a few studies that have addressed coating of small particles from supercritical fluid solutions.[8−11] These studies were focused on the coating of solid particles of pharmaceutical interest. The objective of the current study was to explore supercritical fluids for production of protective polymeric coating on small metal powder particles.

II. Experimental Section

Materials. Aluminum powders (spherical particles of ca. 20 μm in diameter, 99+%, Aldrich) and magnesium powders (325 mesh, 99.5%, Aldrich) were used as substrates. Additional experiments were performed using flat 1 mm thick fused silica substrates to perform

* To whom correspondence should be addressed. E-mail: krasnoperov@adm.njit.edu.

10.1021/ie0100939 CCC: $20.00
Published on Web 08/24/2001

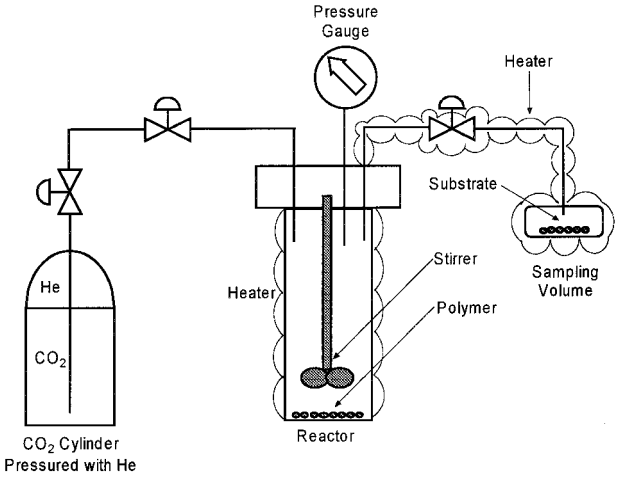

Figure 1. High-pressure temperature-controlled stirred batch reactor with an auxiliary sampling volume.

atomic force microscopy (AFM) and UV characterization of the deposited films.

Two polymers were used to produce protective films: poly(vinylidene fluoride) (PVDF), average $M_w \approx 534\,000$ (Aldrich), and poly(4-vinylbiphenyl) (PVB), average $M_w \approx 115\,000$ (Aldrich).

Common organic solvents were used without additional purification: acetone, 99.5+%, ASC spectrophotometric grade (Aldrich), dichloromethane, 99+%, and *N*,*N*-dimethylformamide, 99.8%, ASC spectrophotometric grade (Aldrich).

Supercritical-grade carbon dioxide (purity 99.99% min, Matheson Co.) was used from cylinders pressurized by helium to 1500 psig. The mole fraction of helium dissolved in CO_2 determined by mass spectrometry was about 2%. The amount of carbon dioxide in the reactor was calculated based on the reactor volume, temperature, and pressure using eq 1:

$$n = pV/ZRT \tag{1}$$

The compression factors for carbon dioxide, *Z*, were taken from standard tables (IUPAC).[31] For comparison, a number of polymer coatings were produced using common organic solvents (acetone, dichloromethane, and *N*,*N*-dimethylformamide).

Experimental Setup and Procedures. The experimental setup is shown in Figure 1. Solutions of polymers in SC CO_2 were prepared in a batch stirred high-pressure temperature-controlled reactor (Autoclave Engineering, BC 0030 SS 05AH, 300 cm^3 volume). Weighed amounts of polymers or aliquots of polymer solutions in dichloromethane of known concentrations were loaded into the reactor. The solvent was removed by flushing the reactor with air. The reactor was sealed and flushed with carbon dioxide to remove air. Then the reactor was filled with carbon dioxide. To obtain the target final pressure at the target temperature of the reactor, carbon dioxide was loaded from the pressurized (85−100 atm) carbon dioxide cylinder at a precalculated initial temperature of the reactor. After the loading, the reactor was heated to the required temperature (in the range 40−300 °C). Temperature was stabilized using a Watlow Parr 4842 temperature controller. To avoid temperature overshot, the heating was performed slowly with a heating rate of ca. 1 °C/min. The reactor was stirred using a magnetic drive stirrer.

Samples of metal powders (usually 200 mg) and/or of fused silica substrates were placed in an auxiliary volume (ca. 5 cm^3) connected to the reactor through a sampling valve. Plane fused silica substrates were used alone or together with the metal powder to produce films for the UV and AFM characterization. The sampling volume was flushed with carbon dioxide to remove air. After flushing, the sampling volume was disconnected from the reactor. The temperature of the sampling volume was controlled independently of the reactor temperature. After the desirable reactor temperature was achieved, the content of the reactor was stirred for ca. 2 h. Then the stirring was stopped, and the mixture in the reactor was allowed to relax (about 10 min; the reactor pressure was recorded at this point).

To perform the film deposition, the sampling valve was opened and the auxiliary volume was connected to the reactor (the pressure change due to the filling the sampling volume when opening the sampling valve was ca. −2%). After ca. 10 min the sampling valve was closed, and the reactor was discharged to the atmosphere. The sampling volume was allowed to cool to 40−70 °C and then discharged.

During the temperature change and the subsequent depressurization, the dissolved polymer precipitates on the internal surface of the auxiliary volume and the sample substrates. It was observed that after the coating procedure the sample powder uniformly covers all of the surface of the sampling volume. This observation suggests the fluidization of the metal powder sample in the auxiliary volume during the filling and the discharge. Such fluidization provides the conditions for the unobstructed particle coating from all sides. The total surface area of the sample particles is ca. 50 times larger than the wall surface area of the sampling volume. Therefore, ca. 98% of the dissolved polymer is expected to precipitate on the surface of the sample powder particles. This was confirmed by direct measurements (see the Results and Discussion section).

In the experiments aimed at the quantitative film thickness characterization, samples of powders coated using polymer solutions with controlled concentrations were prepared using polymer solutions in common solvents. For this purpose, weighed amounts of metal powders were coated with known amounts of polymers dissolved in organic solvents (acetone or dichloromethane) by evaporation of the solvent.

Scanning Electron Microscopy (SEM) and AFM. Images of blank and PVDF-coated aluminum powders were obtained using the Electro Scan 2020 environmental scanning electron microscope (ESEM). The AFM images and profiles of PVDF-coated fused silica plates were obtained using a Digital Instruments Nanoscope IIIa. The AFM was operated in the tapping mode.

Analysis of Samples by UV Spectroscopy. One of the polymers studied, PVB, contains aromatic groups, which have strong absorption bands in the near-UV spectral region. The thicknesses of the PVB films deposited on metal powders were determined using UV absorption spectroscopy. Weighed amounts of coated powders were washed by measured amounts of dichloromethane. The concentrations of the polymers in the solutions obtained were determined using UV absorption spectroscopy. A Varian DMS 300 UV−vis spectrophotometer was used to record the UV absorption spectra.

Measurements of Polymer Solubility in SC CO_2. The solubility of a polymer in SC CO_2 is one of the major properties critical to the process of the film deposition. The majority of the literature data on the polymer solubilities in SC CO_2 were obtained by the cloud-point measurements using mixtures containing relatively large (typically several weight percents[32]) amounts of dissolved polymers. There are only a few data obtained using other techniques.[33] The cloud-point technique is not directly applicable to the moderate and low soluble polymers used in the current study.

Solubilities of low soluble polymers could be determined by measuring a property that reflects the concentration of the polymer in the fluid phase as a function of the reactor load. Before the solubility is reached, the entire loaded amount of the polymer is dissolved, and the concentration in the fluid is proportional to the reactor load. When the solubility is reached, the further increase of the reactor load does not lead to an increase of the polymer concentration in the fluid phase. A property which is sensitive to the concentration of the polymer in the fluid phase (e.g., the deposited film thickness) can serve as an indirect measure of the polymer concentration in the fluid. Before the solubility is reached, the deposited film thickness is expected to increase with the amount of the polymer loaded. After the solubility is reached, no further change in the deposited film thickness with the reactor load is anticipated.

This approach was used to measure the solubility of PVB in SC CO_2. Measured amounts of polymer were loaded in the reactor. Fixed amounts of aluminum powder were loaded in the sampling volume. The PVB film deposition was performed according to the procedure described in the Experimental Setup and Procedures section. The UV absorbance of the organic solutions obtained by washing the samples was measured as a function of the amount of the polymer loaded in the reactor. The absorbance of the solution (proportional to the amount of the washed polymer and, therefore, proportional to the average film thickness) is plotted vs the reactor load. The "break" in the dissolution curve obtained in this way is used to determine the polymer solubility (see the Results and Discussion section).

Dissolution of Metal Powders Coated with Polymers in Alkali and Acids. The evaluation of the protective properties of the deposited polymeric films was performed based on the measurements of the dissolution rates of the powders in basic and acidic solutions.

Aluminum reacts with alkali solutions, forming molecular hydrogen:[34]

$$2Al + 2NaOH + 2H_2O \rightarrow 2NaAlO_2 + 3H_2 \quad (2)$$

Polymer films deposited on the surface of aluminum powder particles decelerate the rate of aluminum dissolution [reaction (2)]. The dissolution reaction (2) was monitored via the mass loss of the powder samples. The reduction of the dissolution "rate constant" of Al powders in the stoichiometric quantities of 0.01 M NaOH solutions upon the film deposition was used as a quantitative measure of the protective properties of the films. In the mass loss monitoring, proper precautions were made to avoid interference from the products of the subsequent transformations of the aluminate ion, AlO_2^-. In aqueous solutions aluminate ion is transformed to the $Al(OH)_4^-$ complex, which is further hydrolyzed, forming insoluble aluminum hydroxide, $Al(OH)_3$.[34] Aluminum hydroxide forms a colloid suspension in the bulk of the solution. To avoid possible errors in the measurements of the mass of the residual aluminum, aluminum hydroxide remained after removal of the major fraction of the original solution was removed through a series of additional washings.

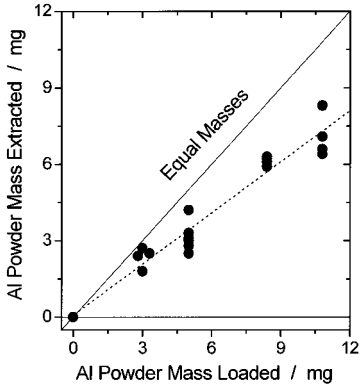

Figure 2. Correction curve for the dissolution kinetics measurements. The mass of extracted aluminum powder (from 40 mL of water, pH 7.0) is plotted vs the mass of the loaded sample. Water was added and removed three times (see text). The dotted line is a linear regression through the experimental points.

In the dissolution kinetic measurements, four to five identical samples of 10.8 mg (4.00×10^{-4} mole of Al) of Al powder were placed in beakers, each containing 40 mL of a 0.01 M NaOH solution (4.00×10^{-4} mol of NaOH). The powders were allowed to dissolve for different periods of time, after which the process of dissolution was terminated by discharging the alkali solutions from the beakers. The powders were washed with water to remove aluminum hydroxide and the residual alkali solutions. For washing, ca. 20 cm^3 of water was added and then removed by a pipet and a syringe from the bulk of the liquid. This procedure was repeated twice. Then the beakers with the residual powder were dried and weighed with and without the residual dry powder to determine the mass of the residual aluminum. The residual mass of the samples was plotted vs the dissolution time.

It was observed, however, that this procedure results in lower masses of aluminum than the loaded amounts even at the zero dissolution time due to the sample loss in the washing procedure. The sample losses are caused both by the removal of a fraction of the aluminum powder with the wash water and by the slow dissolution of aluminum in pure water. The loss in the sample mass is proportional to the loaded amount and was ca. 15% for uncoated and ca. 7% for coated aluminum samples per wash. After discharging the initial solution (which leads to comparable sample losses), the washing procedure was applied two times. To account for the sample losses, correction was introduced into the dissolution experiments by measuring the sample loss with zero dissolution time. The correction curve for the dissolution of the uncoated aluminum powder is shown in Figure 2. The mass of the extracted powder is proportional to the mass of the loaded powder. In the processing of the experimental kinetic curves, the mass of the residual aluminum was multiplied by an empirical correction factor to account for the sample losses. The correction factor for the dissolution of uncoated aluminum powder was 1.47 (Figure 2); the correction factor for the coated powders was 1.21. A smaller correction factor for the

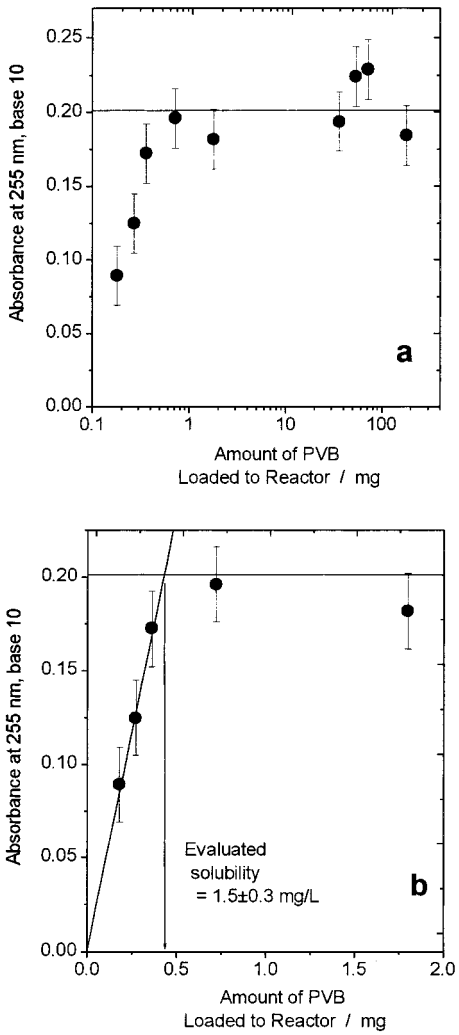

Figure 3. Determination of the solubility of PVB in SC CO_2 at 170 °C and 314 atm. (a) UV absorbance of PVB washed by CH_2Cl_2 from the surface of coated Al powder at 255 nm vs the amount of the polymer loaded in the reactor (logarithmic scale). (b) Initial part of the curve (linear scale). Error bars are ±1 standard deviation of the six points on the plateau.

coated powders is due to the flotation of the coated powders on the liquid surface (see below), which leads to the smaller sample losses during the washing procedure.

Dissolution of magnesium in aqueous NaOH solutions is too slow for the characterization of the film protective properties. For dissolution of magnesium powders, acidic aqueous solutions were used. In sulfuric acid the dissolution of magnesium occurs according to reaction (3):[34]

$$Mg + H_2SO_4 \rightarrow MgSO_4 + H_2 \qquad (3)$$

The product of this reaction, magnesium sulfate, is soluble in water. Therefore, no problem of an insoluble precipitate, such as the one encountered in the dissolution of aluminum powders in alkali solutions, occurs.

III. Results and Discussion

Solubility of PVB in SC CO_2. Determination of the solubility of PVB in SC CO_2 at 170 °C and 314 atm using the approach described in the Experimental Section is shown in Figure 3a (semilog coordinates to incorporate the wide range of the reactor loading used) and Figure 3b (the initial part of the dependence, linear scale). The amount of the polymer transferred and deposited on the sample particles linearly increases with the reactor load until the load of 0.4 mg is reached. Further increase of the reactor load has no effect on the amount of the polymer transferred (the plateau in Figure 3a). The error bars shown in Figure 3 are ±1 standard deviation of the points on the plateau. As follows from the data plotted in Figure 3, at these experimental conditions the solubility of PVB in SC CO_2 is (1.5 ± 0.3) mg/L. This solubility corresponds to the mole fraction of the monomer units of the polymer in SC CO_2 of (7.5 ± 1.5) × 10^{-7}. The measured low value of the solubility of PVB is in accord with the literature data on the low solubility (or almost insolubility) of the lipophilic polymers (such as PVB or polystyrene) in SC CO_2.[35] Nevertheless, even this low solubility of the polymer is sufficient to produce protective films that alter the properties of metal powders.

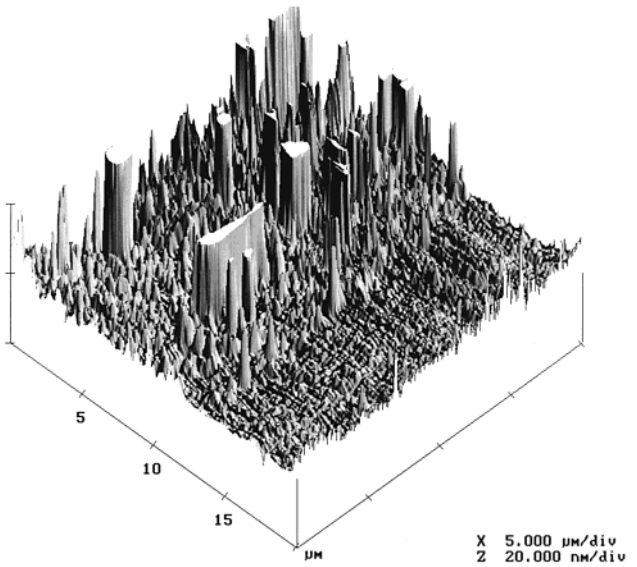

Figure 4. Three-dimensional AFM surface profile of a fused silica plate coated with PVDF at 414 atm and 190 °C from SC CO_2. The scratch (visible in the right-hand side of the picture) was made by a copper needle.

In addition, the amount of the polymer deposited on the surface of the powder was compared with the amount of the polymer transferred to the sampling volume. The latter was calculated based on the mass of the polymer loaded to the reactor (below the solubility limit) and the ratio of the sampling and reactor volumes. The relative fraction of the polymer deposited on the surface of particles was measured as 0.96 ± 0.03 in excellent agreement with that expected from the surface areas (0.98).

Experiments on Coating of Fused Silica Plates with PVDF. To assess the feasibility of the polymer film deposition from SC CO_2, the initial experiments were performed using flat fused silica plates as substrates. These experiments provided visible evidence of the polymer presence on the substrate surface. An AFM three-dimensional topographic image of a fused silica plate coated with PVDF from SC CO_2 is shown in Figure 4. The imaged area of the film contains a scratch made by a copper needle. Two substructures are apparent. The first has the characteristic thickness of a few nanometers and varies on the scale of ca. 1 μm. On the top of this structure, there are much thicker islands

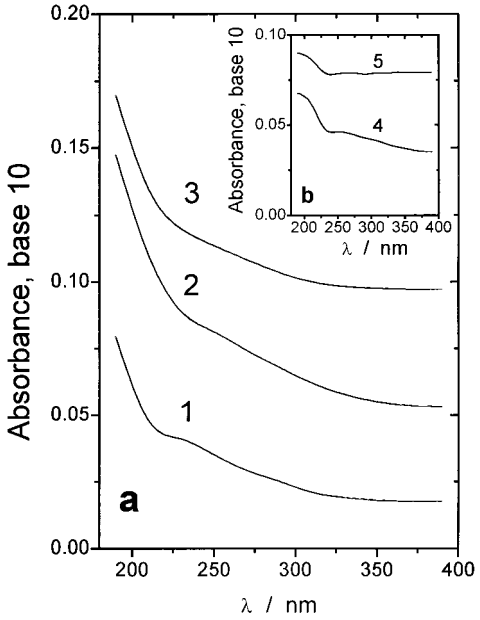

Figure 5. UV light attenuation spectra of PVDF films deposited on fused silica plates. (a) 1: uncoated plate. 2: film prepared by wetting of the surface with a solution of the polymer in acetone and subsequent solvent evaporation. 3: PVDF film deposited from SC CO_2. (b) Light attenuation spectra of the films obtained by subtraction of the light absorption by the fused silica plates (curve 1) from the total light attenuation (curves 2 and 3). Curves 5 and 4 correspond to curves 3 and 2, respectively.

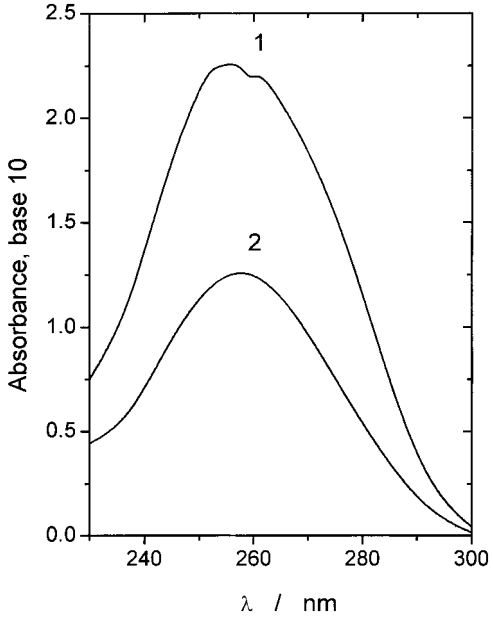

Figure 6. UV absorption spectra of PVB solutions in CH_2Cl_2. The cell length is 1 cm. 1: polymer solution in dichloromethane with the molar concentration of the monomer units of 1.5×10^{-4} M. 2: sample prepared by washing of 124.9 mg of Al powder coated with PVB from SC CO_2 at 220 °C and 372 atm with 2.8 mL of CH_2Cl_2.

with a thickness of more than 20 nm and a spatial scale of ca. 3−5 μm. Although the polymer film is not uniform, it still covers the surface of the substrate, providing protection of the substrate.

Samples of PVDF-coated fused silica substrates were analyzed using UV light attenuation spectra. Figure 5 demonstrates the UV light attenuation spectra by the PVDF films deposited on fused silica plates from both acetone solutions and SC CO_2. In the figure, curve 1 is the light attenuation by an uncoated substrate, curve 2 is the light attenuation by a substrate coated with PVDF from acetone, and curve 3 is the light attenuation by a substrate coated with PVDF using SC CO_2.

Because PVDF has only a weak absorption in the UV region, the observed UV light attenuation is mainly due to the light scattering rather than the light absorption. Under the visual observation of the plates, the light scattering due to the films' unevenness was apparent. The light attenuation spectra (curves 2 and 3 in Figure 5) were interpreted as being due to the light scattering because the curves are structureless (for reference, Figure 6 shows an example of a "structured" UV spectrum formed by a UV absorption band). The light scattering only weakly depends on the wavelength, which indicates the "grain size" to be larger than the wavelengths. This is consistent with the AFM film profile (Figure 4) and the white color of the films.

Films deposited from organic solvents (acetone and *N*,*N*-dimethylformamide) also exhibit a similar light scattering. For these films, the dependence of the light attenuation (monitored at the wavelength of 270 nm) on the average polymer film thickness is shown in Figure 7. Assuming that a similar dependence exists for the films deposited from SC CO_2, the measured films' opacities allow some tentative conclusions on the film thickness dependence on the deposition conditions (such as in Figures 8 and 9). It should be noted, however, that

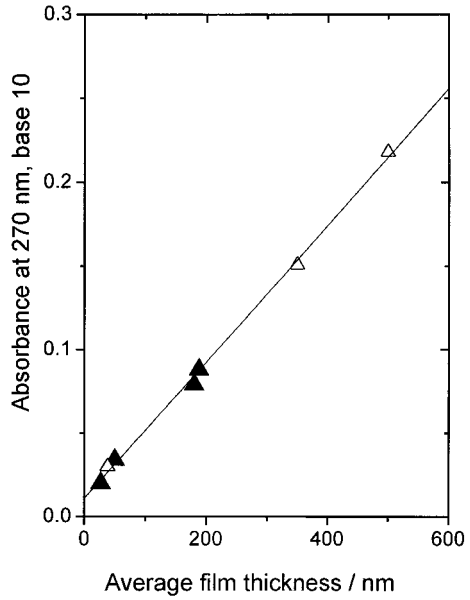

Figure 7. Correlation of the average PVDF film thickness and the UV light attenuation. Films were prepared by wetting of the surface of flat fused silica substrates with a solution of the polymer in acetone (solid triangles) and *N*,*N*-dimethylformamide (open triangles) with the subsequent solvent evaporation. The straight line is a linear regression through the experimental points.

the conclusions derived from Figures 8 and 9 based on the assumption of the monotonic relationship of the film opacity on the film thickness (although confirmed for films prepared using organic solvents) should be considered tentative at best.

The deposition of the polymeric films on fused silica plates located in the sampling volume unambiguously infers the polymer transfer by SC CO_2, because the sampling volume in the experiments was separated from the reactor during heating and stirring and was opened only after the stirring is stopped and the system is allowed some time for relaxation. Polymer transport to

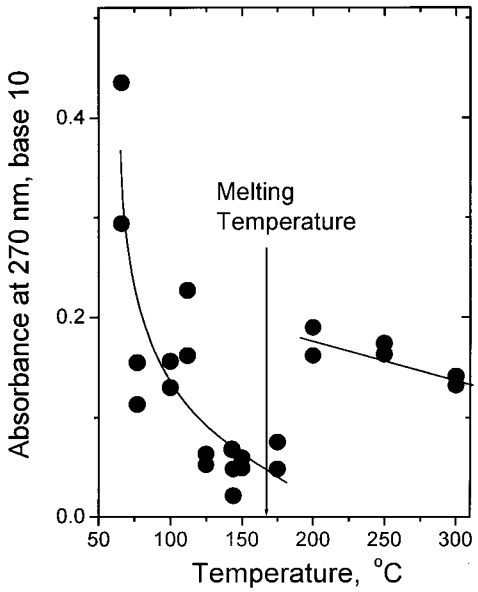

Figure 8. Opacity of the PVDF films deposited on fused silica plates from SC CO_2 at different deposition temperatures. The films opacity was determined via the UV light attenuation at 270 nm. The films were prepared by filling the sampling volume with the polymer solution in SC CO_2 at 200 atm and variable reactor temperature and subsequently cooling the sampling volume to 60 °C and discharging.

the substrate surface may occur either via polymer dissolution in SC CO_2 or through formation of small aerosol-like particles. There is no sharp boundary between these two mechanisms. For example, a single PVDF molecule with a molecular weight of ca. 500 000 would have ca. 45 nm in diameter if a near-spherical particle forms. For the "true dissolution" mechanism, the dissolution curves with sharp "saturation" and no further increase in the amount of the dissolved material after the solubility is reached are anticipated. Such a dissolution curve is shown in Figure 3. For the polymer transfer mechanism via relatively large aerosol-like particles, no sharp change in the amount of the transferred polymer with the reactor load is expected. The observed dissolution curve (Figure 3) indicates the transfer mechanism via the true polymer dissolution (for the specific experimental conditions). It should be noted that the experimental procedure of the current study guarantees precipitation of the polymer particles larger than 3 μm in diameter during the relaxation time. The estimated sedimentation time of these particles is less than 10 min. The sedimentation time of smaller particles (ca. 3 days for 150 nm) is much longer. The contribution of such particles to the polymer transfer could be not ruled out based on the results of the current work.

The experiments with the polymer deposition on fused silica plates were subsequently used to outline the optimal conditions for the film deposition. This study was performed with PVDF. The dependence of the deposited PVDF film opacity at 270 nm on the deposition temperature at a constant pressure of 200 atm is shown in Figure 8. This dependence is nonmonotonic. Initially, the film opacity decreases with the deposition temperature. A sharp increase of the film opacity occurs at ca. 175 °C, which is slightly above the melting point of the polymer. The melting temperature of PVDF is 168 °C; the depression of the melting temperature of the polymer due to SC CO_2 estimated using the results

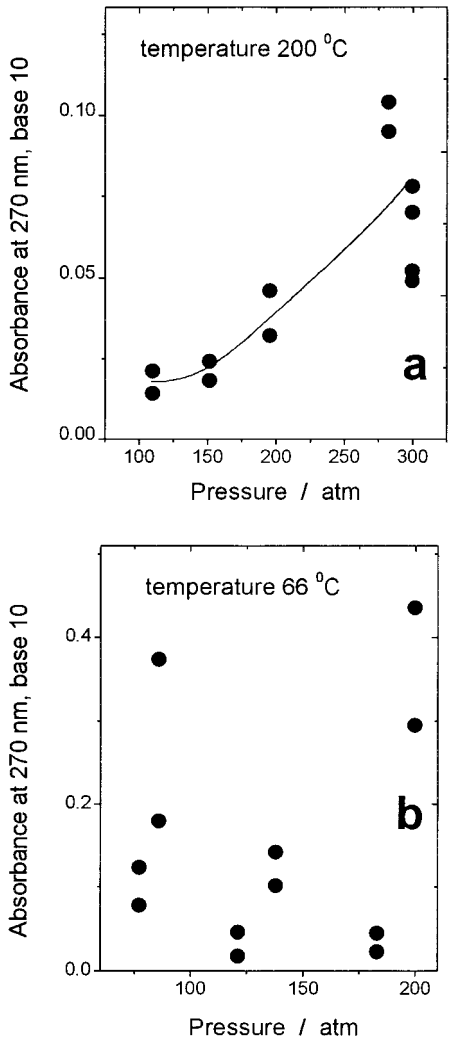

Figure 9. Opacity of PVDF films deposited on fused silica plates from SC CO_2 vs the reactor pressure at constant temperature. The film opacity was determined via the UV light attenuation at 270 nm. (a) Reactor temperature 200 °C. (b) Reactor temperature 66 °C. The sample volume was discharged at 40 °C.

of Dinoia et al.[36] is less than 3 °C at 200 atm of CO_2. The reason for the "jump" of the film opacity near the melting temperature is not established with certainty. One of the possible explanations is in the additional polymer transfer mechanism due to the formation of fine liquid "aerosol" polymeric particles with a long sedimentation time.

Below the melting point of the polymer the decrease in the film opacity with temperature from 66 to 112 °C is observed. This could be due to the temperature dependence of the solubility of the polymer. The effect of temperature on the solubility of solids in supercritical fluids could be both positive and negative.[1,37] The sign of the temperature dependence is controlled by the competition between the two main factors affecting the solubility, the vapor pressure of the solute (which increases with temperature), and the density of the solvent (which decreases with temperature at constant pressure). The sign of the temperature dependence can change with pressure. For the low molecular weight solutes, the change in the sign of the temperature dependence of the solubility with pressure (the "crossover" effect) is known.[32,38−42] For the solutions of polymers in supercritical fluids, both negative and positive effects of temperature on the solubility at

constant pressure were observed.[33,43,44] The results of the experiments shown in Figure 8 can be interpreted as being due to the negative effect of temperature on the solubility of PVDF in SC CO_2 at a pressure of 200 atm. However, for the second polymer used in this study, PVB, the effect of temperature on the solubility at a pressure of 345 atm is positive (see below).

The films deposited at temperatures below the melting point exhibit considerable scattering in the opacity (Figure 8). This could be due to the gas-phase polymer nucleation and cluster formation during the process of the gas discharge from the sampling volume. The films are presumably produced by subsequent agglomeration and precipitation of these clusters leading to the formation of loose and nonuniform films. The films produced at higher temperatures (above the melting point of the polymer) are smoother and more uniform.

The dependencies of the films optical density on the deposition pressure at two temperatures (200 and 66 °C) are shown in Figure 9. The films obtained at 200 °C (above the melting point of the polymer) have better uniformity, as established by visual investigation. At a temperature of 200 °C (Figure 9a), the optical density of PVDF films increases with pressure. At the lower temperature (66 °C, Figure 9b), no certain conclusion on the pressure dependence could be derived because of the large scatter of the experimental points.

It is stated in the literature that under the experimental conditions used in this work PVDF is "insoluble" in SC CO_2[35,36] in apparent contradiction with the current experimental results. The sensitivity of the method used in the cited works[35,36] is limited to relatively high solubilities. The method used[35,36] is based on the measurements of the cloud formation point in polymeric solutions in SC CO_2 using a view cell.[45] The loaded amounts of polymers were large (0.2−0.7 g of polymer/8−16 g of CO_2). The technique is limited to relatively high solubilities and cannot detect lower solubilities typical for the polymers used and the experimental conditions in the current work. In this work, the estimated weight fraction of PVB dissolved in SC CO_2 at 200 bar and 250 °C is 0.02%, which is only about 2% of the weight fractions of polymers used in the cited works.[35,36] In other words, the cloud-point technique[45] was not sensitive enough to measure the lower solubilities of the polymers used in the current work. The solubility of PVDF in SC CO_2 being much smaller compared to the other polymers studied by the cloud-point technique[35] [polyacrylates, poly(vinyl acetate), and some fluorinated copolymers] is still sufficient to produce protective polymeric films on the surfaces of solid substrates.

Determination of the Average Film Thickness on Powders Using UV Spectroscopy. For PVB (which exhibits strong absorption in the near-UV spectral region) UV spectroscopy was used to estimate the total amount of polymer deposited on the surface of the particles. The total amount of the deposited polymer was used to calculate the average film thickness. The average film thickness was correlated with the protective properties of the polymeric films (see below).

UV absorption spectra of PVB obtained as outlined in the Experimental Section are shown in Figure 6. The spectrum of PVB washed from Al powder coated in SC CO_2 is shown together with the reference spectrum of the polymer dissolved in CH_2Cl_2. The two spectra are similar (a small, ca. 1 nm, shift of the absorption maximum and a small deformation of the absorption band shape are, probably, due to the partial polymer modification in the reactor). The absorption parameters of PVB solutions in dichloromethane (the wavelength of the maximum absorption 255 nm and the maximum molar absorption per monomer 15 600 M^{-1} cm^{-1}) were used to determine the average film thickness. Weighed samples of coated powders were washed with measured volumes of dichloromethane. The average thickness of the polymer film, d, was calculated using eq 4:

$$d = \frac{M_{\text{mono}} D V_{\text{solv}}}{\epsilon_{\text{mono}} l m_{\text{S}} S_{\text{m}} \rho_{\text{poly}}} \tag{4}$$

In this equation, M_{mono} is the molar mass of the monomer unit of the polymer, D is the absorbance of the polymer solution (base 10), V_{solv} is the solvent volume used to wash the sample, ϵ_{mono} is the molar absorbance of the polymer per monomer unit (base 10), l is the length of the absorption cell, m_{S} is the mass of the sample of the coated substrate, S_{m} is the surface of substrate particles per unit mass of the powder, and ρ_{poly} is the polymer density. For spherical, 20 μm in diameter, Al particles, $S_{\text{m}} = 1110$ cm^2/g.

To evaluate the impact of the nonspherical shape and the dispersion of particle size on the calculated average film thickness, the SEM image of the powder was analyzed. A typical SEM picture of the aluminum powder is shown in Figure 10. The sizes of 100 particles were measured. The powder particles are approximately prolate ellipsoids with axes of 20.2 ± 8.2 and 26.8 ± 11.8 μm. The surface per unit of mass is $S_{\text{m}} = 1170 \pm 470$ cm^2/g. The uncertainty in the film thickness caused by neglecting the nonspherical shape and the dispersion of the particle size in eq 4 is estimated as ±40%.

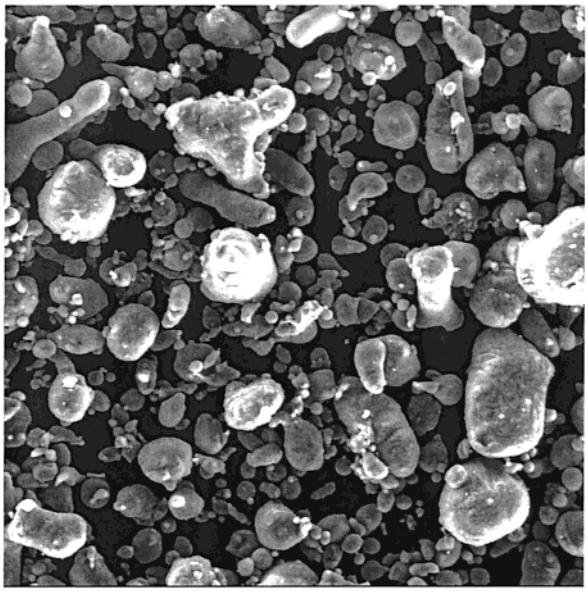

Figure 10. ESEM image of the blank aluminum powder used in the current work.

An example of a SEM picture of PVDF-coated aluminum powder is shown in Figure 11b. Typical average thicknesses of the films deposited on metal powders from SC CO_2 in the current study were in the range of 1−30 nm. The average film thickness of the sample

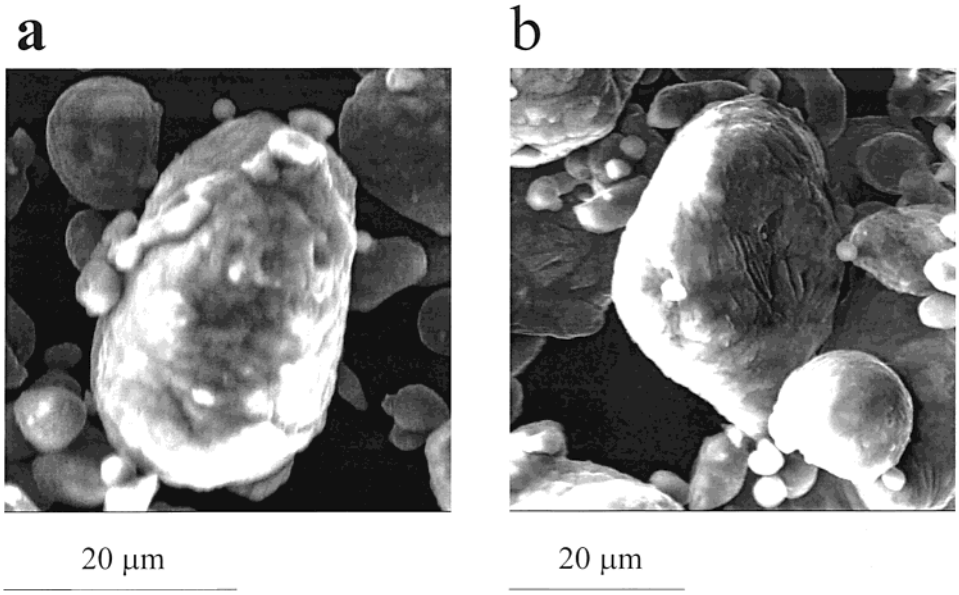

Figure 11. ESEM images of blank (a) and PVDF-coated (b) (SC CO_2, reactor conditions 190 °C, 414 atm) aluminum particles. The film is too thin (the estimated average thickness is ca. 70 nm) to make noticeable differences in the SEM images.

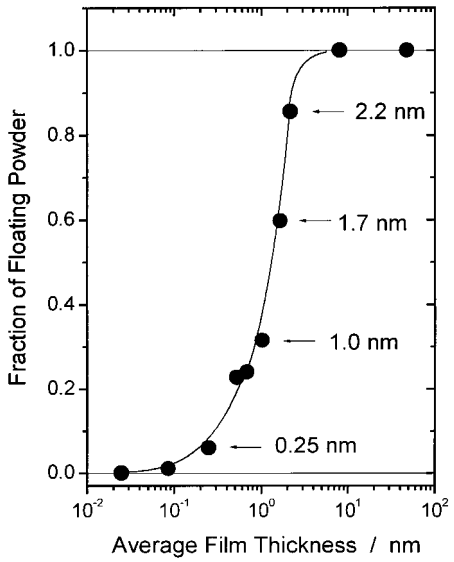

Figure 12. Flotation of Al powder coated with PVDF on the water surface. The mass fraction of the floating powder is plotted vs the average film thickness. 0: all powder sinks. 1: all powder floats.

shown in Figure 11b is ca. 70 nm. Still, the film is too thin to make noticeable differences in the SEM images of the blank (Figure 11a) and coated (Figure 11b) particles. Better results were obtained using AFM profilometry (Figure 4).

Flotation of Coated Al Powder on the Water Surface. Metal particles coated with polymeric films both from SC CO_2 and organic solvents float on the surface of water. This can be used as a simple test on the presence of a polymeric film. Coated powders float on the surface of water, while blank (uncoated) powders sink. To evaluate this effect quantitatively, additional experiments were performed with powders coated with PVDF using acetone solutions with controlled concentrations of the polymers. Figure 12 illustrates the dependence of the mass fraction of floating Al powder particles coated with PVDF on the average polymer film thickness. Approximately 50% of the powder particles float when the average polymer thickness is ca. 1.3 nm, which corresponds to the average coverage of 2.8 monolayers of the monomer. The thickness of the monolayer was estimated as the diameter of a spherical-shape monomer unit of the polymer. Calculations using both the molar volume of the monomer units of the polymer and the summation of the van der Waals group increments[46] result in close values of the monomer diameter (0.48 and 0.43 nm, respectively).

Protective Properties of Polymer Films. One of the practically important properties of the coated metal powders is the increase of their resistance to aggressive media. The coating decelerates the rate of the dissolution of metal powders in basic or acidic aqueous solution up to an order of magnitude. The effects of the PVDF coatings produced from acetone as well as from SC CO_2 on the dissolution rate of aluminum powder in an alkali solution are shown in Figure 13. Films produced using both SC CO_2 and the organic solvent show comparable protection. Figure 14 demonstrates the protective action of the PVDF coatings on magnesium powders monitored by the dissolution in sulfuric acid.

The experimental dissolution curves are satisfactorily fitted by the "second-order" kinetic law (eq 5; Figures 13 and 14):

$$m(t) = m_0/(1 + k_2 t) \qquad (5)$$

where $m(t)$ is the mass of the powder at time t, m_0 is the initial mass, and k_2 is the apparent rate constant-.There is no fundamental justification for eq 5. It was empirically found that the experimental data could be satisfactory fitted by eq 5.

Dissolution of uncoated magnesium powder in sulfuric acid (reaction 3) is about 2 orders of magnitude faster than the dissolution of aluminum powders in alkali solutions. This is not convenient for quantitative measurements. For this reason, only a few experiments were performed with magnesium powders. In the majority of the experiments, aluminum was used as a substrate material to characterize the protective properties of the produced films via dissolution in alkali.

The measurements of the dissolution rates were performed both with and without the forced stirring of the reacting mixture. When no additional stirring was

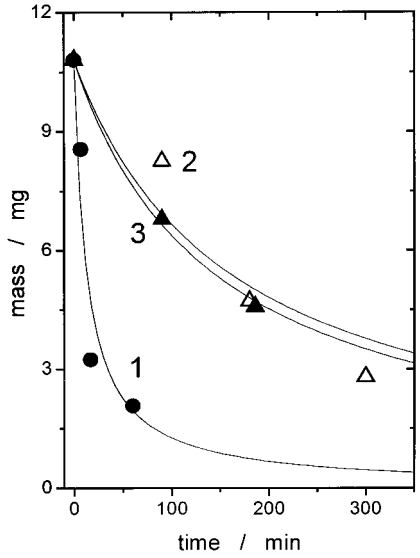

Figure 13. Dissolution of Al powders in NaOH aqueous solutions. 1: uncoated powder. 2: powder coated with PVDF from SC CO_2 (250 °C, 200 atm). 3: powder coated with PVDF from a solution in acetone. The initial mass of the powder was 10.8 mg. 40 mL of 0.01 M NaOH solution (stoichiometric quantities, no magnetic bar stirring). Symbols: experiment. Solid lines: "second-order" fits (see text). The dissolution "rate constants" are $(7.6 \pm 2.4) \times 10^{-2}$, $(7.0 \pm 0.3) \times 10^{-3}$, and $(6.2 \pm 1.4) \times 10^{-3}$ min^{-1} for curves 1−3, respectively.

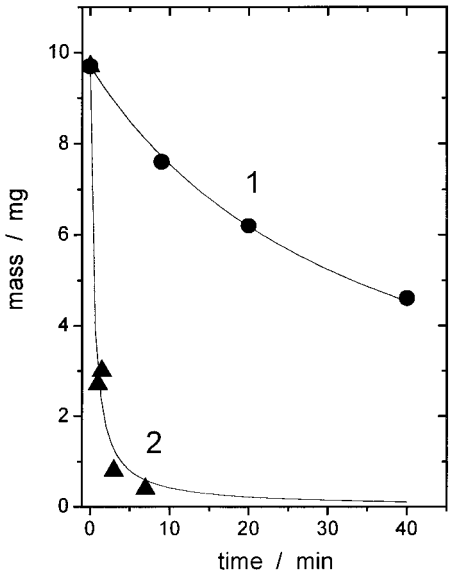

Figure 14. Dissolution of Mg powders in a H_2SO_4 aqueous solution. 1: uncoated powder. 2: powder coated with PMMA from SC CO_2 (170 °C, 303 atm). The initial mass of the powders was 9.7 mg. 40 mL of 0.01 M H_2SO_4 (stoichiometric quantities). No magnetic bar stirring. Symbols: experiment. Solid lines: "second-order" fits (see text). The "rate constants" are 2.2 ± 0.4 and 0.028 ± 0.001 min^{-1} for curves 1 and 2, respectively.

applied, there still was some mixing of the "reaction mixture" caused by the convection induced by the evolving molecular hydrogen. The impact of the forced stirring on the apparent dissolution rate constant is shown in Figure 15. Forced stirring accelerates dissolution of uncoated aluminum powders by a factor of ca. 1.5. For coated powders, which float on the surface of the solution, the increase in the dissolution rate under forced stirring can reach a factor of 3.

The ratio of the dissolution rate constants for the coated and uncoated (blank) powders was used as a

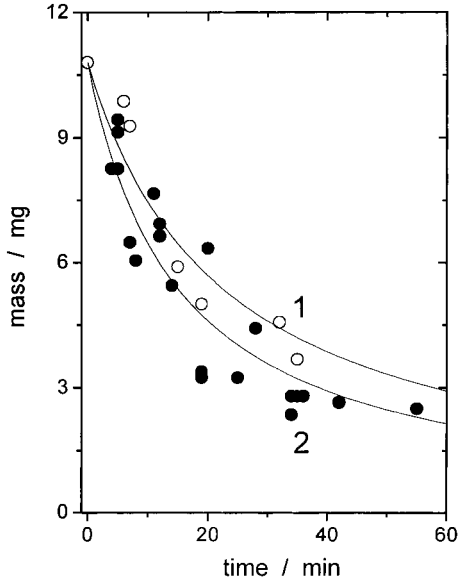

Figure 15. Effect of the solution stirring with a magnetic bar on the rate of dissolution of blank aluminum powder in a NaOH aqueous solution. A sample of 10.8 mg of uncoated aluminum powder in 40 mL of 0.01 M NaOH. Points: experiment. Lines: "second-order" fit (see text). 1: no stirring. 2: stirring with a magnetic bar. The dissolution "rate constants" are $(4.5 \pm 0.7) \times 10^{-2}$ and $(6.7 \pm 0.6) \times 10^{-2}$ min^{-1} for curves 1 and 2, respectively.

quantitative measure of the polymer film protective properties. For example, Figure 13 illustrates ca. 10 times slower dissolution of the coated powder compared with the uncoated sample. Similar protection properties were observed for both polymers studied in this work.

Two mechanisms could be partially responsible for the observed deceleration of the dissolution of coated metal powders in acidic and basic solutions. First, polymer films prevent direct contact between the metal and the liquid phase. Second, because of the flotation of coated particles on the surface, the efficiency of the reactant mixing induced by evolving hydrogen is diminished, which could have an effect on the dissolution rate. The impacts of both mechanisms on the total protection effect were verified experimentally. A sample of aluminum powder coated with PVDF in SC CO_2 was forced into the bulk in a completely closed vessel filled with an aqueous NaOH solution; all of the powder particles sank. The dissolution of aluminum in this experiment was ca. 40% faster than the dissolution of a floating sample, but still ca. 2 times slower than that of blank aluminum powder (all experiments without stirring). Therefore, the observed deceleration of the powder dissolution is only partially due to the powder flotation. There is an "intrinsic" protection provided by the films similar to that provided by the native metal oxide film on the particle surface.

Figure 16 shows the dependence of the dissolution rate of Al powders coated by PVDF on the pH of the solution. The dissolution rate has a minimum in neutral solutions (pH = 7.0). The rate of dissolution increases in both acidic and basic solutions. The dependence of the dissolution rate on pH is almost symmetric relative to the neutral pH (7.0). A similar behavior is observed in corrosion of aluminum.[47]

The protective properties of the polymer films deposited from SC CO_2 depend on the coating conditions. Figure 17 shows the correlation between the deposition temperature, the average film thickness, and the protective properties of PVB films deposited on aluminum

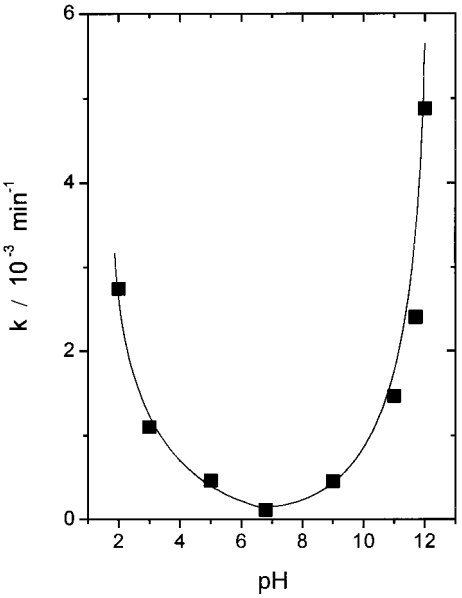

Figure 16. Effect of pH on the dissolution rate of the PVDF-coated (SC CO_2, 200 °C, 310 atm) aluminum powders in basic (NaOH) and acidic (HCl) aqueous solutions. No magnetic bar stirring. Symbols: experiment. Solid line: spline through the experimental points.

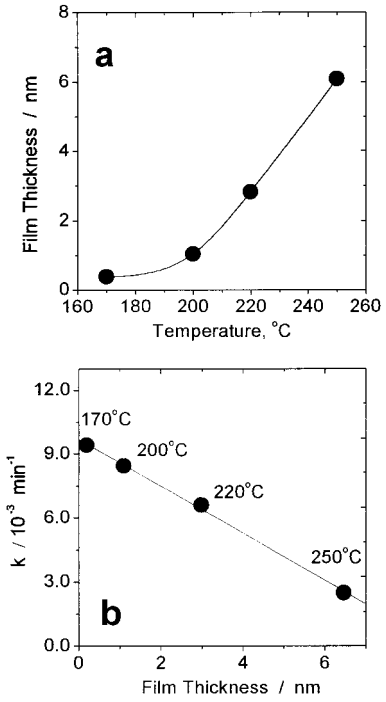

Figure 17. Correlation of the dissolution rate constant and the film thickness for the films prepared at different reactor temperatures. Reactor pressure 345 atm. (a) Average film thickness vs deposition temperature. (b) Dissolution rate constant of PVB-coated Al powders in NaOH (0.01 M, no magnetic bar stirring) vs the average film thickness. Symbols: experiment. Solid lines: spline (a) and linear regression (b). The reactor temperatures are indicated in the figure.

powder at 345 atm. The dependence of the PVB film thickness on the deposition temperature is shown in Figure 17a. The thickness of the films deposited at 170 °C is ca. 0.4 nm, which is close to the thickness of a monolayer. Increasing the temperature to 250 °C results in a 16-fold increase in the film thickness. The dependence of the film protective properties on the film thickness (varied by changing the deposition temperature) is shown in Figure 17b. The dissolution rate decreases with an increase of the mean film thickness. Hence, for the PVB deposition at 345 atm, the higher deposition temperatures result in thicker polymeric films with better protective properties.

IV. Conclusions

Thin polymeric films were deposited on flat fused silica substrates as well as metal powders using SC CO_2 as a solvent. The average film thickness was determined using UV absorption of the solution produced by dissolution of the deposited polymers with an organic solvent. The protection properties of the films were quantified via the monitoring of the powder dissolution kinetics in basic and acidic aqueous solutions. Polymeric films deposited from SC CO_2 exhibit substantial protective properties even for polymers with very low solubility.

A method to measure the solubilities of the low soluble polymers in SC CO_2 was developed. The solubility of PVB in SC CO_2 was determined. The solubility (defined as the mole fraction of the monomer units of the polymer) is $(7.5 \pm 1.5) \times 10^{-7}$ at a temperature of 170 °C and a pressure of 314 atm. Evaluation of the properties of the films prepared by deposition of 11 different polymers from SC CO_2 as well as common organic solvents is in progress.

Acknowledgment

The work was supported by the U.S. Army Sustainable Green Manufacturing Program.

Literature Cited

(1) Savage, P. E.; Gopalan, S.; Mizan, T. I.; Martino, C. J.; Brock, E. E. Reactions at Supercritical Conditions: Applications and Fundamentals. *AIChE J.* **1995**, *41*, 1723.

(2) Kim, S.; Johnston, K. P. Effects of Supercritical Solvents on the Rates of Homogeneous Chemical Reactions. In *Supercritical Fluids*; Squires, T. G., Paulaitis, M. E., Eds.; ACS Symposium Series 329; American Chemical Society: Washington, DC, 1987; p 42.

(3) McHuge, M.; Krukonis, V. *Supercritical Fluid Extraction*, 2nd ed.; Butterworth-Heinemann: Boston, 1994.

(4) Henon, F. E.; Camaiti, M.; Burke, A. L. C.; Carbonell, R. G.; DeSimone, J. M.; Piacenti, F. Supercritical CO_2 as a Solvent for Polymeric Stone Protective Materials. *J. Supercrit. Fluids* **1999**, *2*, 173.

(5) Brennecke, J. F.; Chateaneuf, J. E. Homogeneous Organic Reactions as Mechanistic Probes in Supercritical Fluids. *Chem. Rev.* **1999**, *99*, 433.

(6) Cooper, A. I.; DeSimone, J. M. Polymer Synthesis and Characterization in Liquid and Supercritical Carbon Dioxide. *Curr. Opin. Solid State Mater. Sci.* **1996**, *1*, 761.

(7) Cooper, A. I. Synthesis and Processing of Polymers using Supercritical Carbon Dioxide. *J. Mater. Chem.* **2000**, *10*, 207.

(8) Tom, J. W.; Debenedetti, P. G.; Jerome, R. Precipitation of Poly(L-lactic acid)−Pyrene Particles by Rapid Expansion of Supercritical Solutions. *J. Supercrit. Fluids* **1994**, *7*, 9.

(9) Tom, J. W.; Lim, J.-B.; Debenedetti, P. G.; Prud'homme, R. K. Applications of Supercritical Fluids in the Controlled Release of Drugs. In *Supercritical Fluids Engineering Science. Fundamentals and Applications*; Kiran, E., Brennecke, J. F., Eds.; ACS Symposium Series 514; American Chemical Society: Washington, DC, 1993; p 238.

(10) Kim, J.-H.; Paxton, T. E.; Tomasko, D. L. Microencapsulation of Naproxene using Rapid Expansion of Supercritical Solutions. *Biotechnol. Prog.* **1996**, *12*, 650.

(11) Mishima, K.; Matsuyama, K.; Tanabe, D.; Satoru, Y.; Young, T. J.; Johnston, K. P. Microencapsulation of Proteins by Rapid Expansion of Supercritical Solution with a Nonsolvent. *AIChE J.* **2000**, *46*, 857.

(12) Elvers, B., Hawkins, S., Russey, W., Shulz, G., Eds. *Ullman's Encyclopedia of Industrial Chemistry*, 5th ed.; VCH: Weinheim, Germany, 1993; Vol. A22.

(13) Gotoh, K., Masuda, H., Higashitani, K., Eds. *Powder Technology Handbook*, 2nd ed.; Marcel Dekker Inc.: New York, 1999.

(14) Renner, R. H.; Farncomb, R. E.; Nauflett, G. W.; Deiter, S. J. Characterization of MTV Made by the Shock Gel Process. *Int. Symp. Energetic Mater. Technol.* **1995**, *680*, 174.

(15) Shelukar, S.; Ho, J.; Zega, J.; Roland, E.; Yeh, N.; Quiram, D.; Nole, A.; Katdare, A.; Reynolds, S. Identification and Characterization of Factors Controlling Tablet Coating Uniformity in a Wurster Coating Process. *Powder Technol.* **2000**, *110*, 29.

(16) Sudsakorn, K.; Turton, R. Nonuniformity of particle Coating on a Cise Distribution of Particles in a Fluidized Bed Coater. *Powder Technol.* **2000**, *110*, 37.

(17) Hannay, J. B.; Hogarth, J. On the Solubility of Solids in Gases. *Proc. R. Soc. London* **1879**, *29*, 324.

(18) Paulaitis, M. E.; Krukonis, V. J.; Kurnik, R. T.; Reid, R. C. Supercritical Fluids Extraction. *Rev. Chem. Eng.* **1983**, *1*, 179.

(19) McHuge, M.; Krukonis, V. *Supercritical Fluid Extraction*; Butterworth: Boston, 1986.

(20) Larson, K. A.; King, M. L. Evaluation of Supercritical Fluid Extraction in the Pharmaceutical Industry. *Biotechnol. Prog.* **1986**, *2*, 73.

(21) Ma, X.; Tomasko, D. L. Coating and Impregnation of a Nonwoven Fibrous Polyethylene Material with a Nonionic Surfactant using Supercritical Carbon Dioxide. *Ind. Eng. Chem. Res.* **1997**, *36*, 1586.

(22) Petersen, R. C.; Matson, D. W.; Smith, R. D. Rapid Expansion of Low Vapor Pressure Solid in Supercritical Fluid Solutions: the Formation of the Films and Powders. *J. Am. Chem. Soc.* **1986**, *108*, 2100.

(23) Matson, D. W.; Fulton, J. L.; Petersen, R. C.; Smith, R. D. Rapid Expancion of Supercritical Fluid Solutions: Solute Formation of Powders, Thin Films, and Fibers. *Ind. Eng. Chem. Res.* **1987**, *26*, 2298.

(24) Mohamed, R. S.; Debenedetti, P. G.; Prud'homme, R. K. Effect of Process Conditions on Crystals Obtained from Supercritical Mixtures. *AIChE J.* **1989**, *35*, 325.

(25) Chang, C. J.; Randolph, A. D. Precipitation of Microsize Organic Particles from Supercritical Fluids. *AIChE J.* **1989**, *35*, 1986.

(26) Tom, J. W.; Debenedetti, P. G. Formation of Bierodible Polymeric Microspheres and Microparticles by Rapid Expansion of Supercritical Solutions. *Biotechnol. Prog.* **1991**, *7*, 403.

(27) Adshira, T.; Kanazawa, K.; Arai, K. Rapid and Continuous Hydrothermal Crystallization of Metal Oxide Particles in Supercritical Water. *J. Am. Ceram. Soc.* **1992**, *75*, 1019.

(28) Adshira, T.; Kanazawa, K.; Arai, K. Rapid and Continuous Hydrothermal Synthesis of Bohemite Particles in Subcritical and Supercritical Water. *J. Am. Ceram. Soc.* **1992**, *75*, 2615.

(29) Mawson, S.; Johnston, K. P.; Combes, J. R.; DeSimone, J. M. Formation of Poly(1,1,2,2-tetrahydroperfluorododecyl acrylate) Submicron Fibers and Particles from Supercritical Carbon Dioxide Solution. *Macromolecules* **1995**, *28*, 3182.

(30) Shim, J.-J.; Yates, M. Z.; Johnston, K. P. Polymer Coatings by Rapid Expansion of Suspensions in Supercritical Carbon Dioxide. *Ind. Eng. Chem. Res.* **1999**, *38*, 3655.

(31) Angus, S., Armstrong, B., de Reuck, K. M., Eds. *International Thermodynamic Tables of the Fluid State*: *Carbon Dioxide*; Pergamon Press: Oxford, 1976.

(32) Yamini, Y.; Bahramifar, N. Solubility of Polycyclic Aromatic Hydrocarbons in Supercritical Carbon Dioxide. *J. Chem. Eng. Data* **2000**, *45*, 53.

(33) Dimitrov, K.; Boyadzhiev, L.; Tufeu, R.; Cansell, F.; Barth, D. Solubility of Poly(ethylene glycol) Nonyphenyl Ether in Supercritical Carbon Dioxide. *J. Supercrit. Fluids* **1998**, *14*, 41.

(34) Durrant, P. J.; Durrant, B. *Introduction to Advanced Inorganic Chemistry*; Wiley and Sons Inc.: New York, 1962.

(35) Rindfleich, F.; Dinoia, T. P.; McHugh, M. A. Solubility of Polymers and Copolymers in Supercritical CO_2. *J. Phys. Chem.* **1996**, *100*, 15581.

(36) Dinoia, T. P.; Conway, S. E.; Lim, J. S.; McHugh, M. A. Solubility of Vinylidene Fluoride Polymers in Supercritical CO_2 and Halogenated Solvents. *J. Polym. Sci. B* **2000**, *38*, 2832.

(37) Bartle, K. D.; Clifford, A. A.; Jafar, S. A.; Shilstone, G. F. Solubilities of Solids and Liquids of Low Volatility in Supercritical Carbon Dioxide. *J. Phys. Chem. Ref. Data* **1991**, *20*, 713.

(38) Diepen, G. A. M.; Schleffer, F. E. C. The Solubility of Naphthalene in Supercritical Ethylene. *J. Am. Chem. Soc.* **1948**, *70*, 4085.

(39) Tsekanskaya, Y. V.; Iomtev, M. B.; Mushkina, E. V. Solubility of Diphenylamine and Naphthalene in Carbon Dioxide under Pressure. *Russ. J. Phys. Chem.* **1962**, *38*, 1173.

(40) McHugh, M.; Paulaitis, M. E. Solid Solubilities of Naphthalene and Biphenyl in Supercritical Carbon Dioxide. *J. Chem. Eng. Data* **1980**, *25*, 326.

(41) Johnston, K. P.; Barry, S. E.; Read, N. K.; Holcomb, T. R. Separation of Isomers Using Retrograde Crystallization from Supercritical Fluids. *Ind. Eng. Chem. Res.* **1987**, *26*, 2372.

(42) Foster, N. R.; Gurdal, G. S.; Yun, J. S. L.; Liong, K. K.; Tilly, K. D.; Ting, S. S. T.; Singh, H.; Lee, J. H. Significance of the Crossover Pressure in Solid-Supercritical Fluid Phase Equilibria. *Ind. Eng. Chem. Res.* **1991**, *30*, 1955.

(43) Kirby, C. F.; McHuge, M. A. Phase Behavior of Polymers in Supercritical Fluid Solvents. *Chem. Rev.* **1999**, *99*, 565.

(44) Kiran, E.; Zhuang, W. Miscibility and Phase Separation of Polymers in Near- and Supercritical Fluids. In *Supercritical Fluids*: *Extraction and Pollution Prevention*; Abraham, M. A., Sunol, A. K., Eds.; ACS Symposium Series 670; American Chemical Society: Washington, DC, 1996; p 2.

(45) Meilchen, M. A.; Hasch, B. M.; McHugh, M. A. Effect of Copolymer Composition on the Phase Behavior of Mixtures of Poly(ethylene-*co*-methyl acrylate) with Propane and Chlorodifluoromethane. *Macromolecules* **1991**, *24*, 4874.

(46) Edward, J. T. Molecular Volumes and the Stokes−Einstein Equation. *J. Chem. Ed.* **1970**, *47*, 261.

(47) Talbot, D.; Talbot, J. *Corrosion Science and Technology*; CRC Press: Boca Raton, FL, 1998.

Received for review January 26, 2001
Revised manuscript received June 7, 2001
Accepted June 21, 2001

IE0100939